Conformal Electrodeposition of Ultrathin Polymeric Films with Tunable Properties from Dual-Functional Monomers

Journal:	*Molecular Systems Design & Engineering*
Manuscript ID	ME-ART-11-2022-000246.R1
Article Type:	Paper
Date Submitted by the Author:	01-Feb-2023
Complete List of Authors:	Wang, Wenlu; Boston University, Material Science and Engineering Zheng, Zhaoyi; Boston University, Resing, Anton; Boston University, Materials Science and Engineering Brown, Keith; Boston University, Mechanical Engineering Werner, Jörg; Boston University, Mechanical Engineering

Design, system, application statement

Functional coatings and interphases influence the stability and performance parameters of electrodes in applications ranging from energy storage and conversion to sensing by controlling molecular and ionic transport to and from surfaces. Polymer thin films offer a wide range of molecular structures and compositions for tunable selectivity and permeability that can be custom designed to the needs of an application. While coating methods on planar substrates are well established, emerging functional materials with 3D architectures and complex porosity present challenges to obtaining conformal polymer thin films on their interior surface with traditional line-of-sight deposition methods. Here, we report a molecular design concept of dual-functional molecules that contain electrochemically active end groups for self-limiting electropolymerization, and a core molecular motif that determines the thin film functionality. The electrodeposition of this monomer represents a non-line-of-sight coating method for polymer thin films on conductive substrates with arbitrary shape. Specifically, we synthesized triethylene glycol diphenol as a dual-functional monomer and studied its electrodeposition, revealing a large tunability window of its molecular permeability and thickness on the nanoscale. We demonstrate its passivating deposition on 3D-structured electrodes that could enable molecular control over interfacial mass transfer in batteries.

ARTICLE

Conformal Electrodeposition of Ultrathin Polymeric Films with Tunable Properties from Dual-Functional Monomers

Received 00th January 20xx,
Accepted 00th January 20xx

DOI: 10.1039/x0xx00000x

Wenlu Wang[1], Zhaoyi Zheng[1], Anton B. Resing[1], Keith A. Brown[1,2,3], Jörg G. Werner[1,2*]

Functional thin films and interphases are omnipresent in modern technology and often determine the performance and lifetime of devices. However, existing coating strategies are incompatible with emerging mesoscaled 3D architected and porous materials, and fail to uniformly apply functional thin films on their large and complex interior 3D surface. In this report, we introduce an approach for obtaining conformal polymeric thin films using custom-designed dual-functional monomers possessing both self-limiting electrodeposition capability and the functionality of interest in separate molecular motifs. We exemplify this approach with the monomer triethylene glycol-diphenol and demonstrate the full coating of a 3D mesoscaled battery electrode with an ultrathin lithium-ion permeable film. Our comprehensive study of the processing-structure-property relationships enables the tailorable control over the conformal thickness (7-80 nm), molecular permeability, and electronic properties. The modularity and tunability of this approach make it a promising candidate for functional polymer film deposition on arbitrary 3D structures.

Introduction

Over the past decades, functional thin-film coatings on planar and macroscale structures have been technology-enabling and performance-determining in applications from electronics to simple commodities such as sunglasses.[1-4] Polymer thin films in particular play a critical role in modern society thanks to a wide range of tunable properties determined by their molecular architecture and composition.[5,6] While polymer thin film fabrication is well-established for the "outside" of materials, the emergence of architected metamaterials and precise multifunctional composites with mesoscale 3D architectures and complex porosity necessitate new synthesis and deposition paradigms for their "interior" surfaces.[7-9] The realization of such 3D conformal interphases that combine the versatility and tunability of polymer functionality with the high surface area of 3D mesoscaled architectures promises new discoveries and could enable unprecedented advances in optical metamaterials,[10,11] energy storage,[12,13] catalysis,[14,15] and mechanical metamaterial actuators.[16]

A limited number of polymer deposition methods are aimed at non-planar thin films: Coatings from initiated chemical vapor phase deposition (CVD) are conformal on low aspect-ratio non-planar substrates, but restricted mass transport and competing side reactions result in limitations in mesoscale 3D structures with nano- and micrometer pore sizes or high aspect ratios.[17] Grafting has been successfully applied to obtain polymer brushes on a variety of materials with complex architectures, but its sensitivity to surface functionality renders it unsuitable for heterogeneous materials and coatings are limited to (macro)molecular monolayers.[18-20] So far, solely the layer-by-layer (LbL) deposition of polyelectrolytes produces polymer thin films on arbitrary substrate shapes with remarkable control over the submicron film thickness.[21-23] However, LbL is limited to hydrophilic polymers since the deposition mechanism requires a large fraction of charged monomers or strong hydrogen bonding, a sometimes undesirable coupled processing-property relationship.[24]

One approach to a versatile functional coating method for 3D materials is to separate the deposition chemistry from the thin film functionality. With regard to the former, electrodeposition of insulating materials is promising for the fabrication of uniform thin films regardless of the substrate architecture due to the surface confinement of the charge-transfer reaction and its self-limiting nature.[25,26] Electropolymerization of phenolic derivatives to poly(phenylene oxide) (PPO) in particular has been successfully employed for nano-scale polymer coatings in corrosion protection, electrochemical sensors, and advanced energy-storage devices, though with limited functionality and tunability of the film itself.[13,27-31] Hence, we propose that the rational design of monomers containing one motif for electropolymerization and one that defines the thin film properties yields a non-line-of-sight deposition method of mesoscaled conformal polymer coatings with independently tailored functionalities on conductive substrates of arbitrary shape and heterogenous surface activity, as has been demonstrated for molecular monolayers from electrolgrafting.[32]

[a.] Division of Materials Science and Engineering, Boston University, Boston, MA 02215, USA.
[b.] Department of Mechanical Engineering, Boston University, Boston, MA 02215, USA
[c.] Department of Physics, Boston University, Boston, MA 02215, USA.
† Footnotes relating to the title and/or authors should appear here.
Electronic Supplementary Information (ESI) available: [details of any supplementary information available should be included here]. See DOI: 10.1039/x0xx00000x

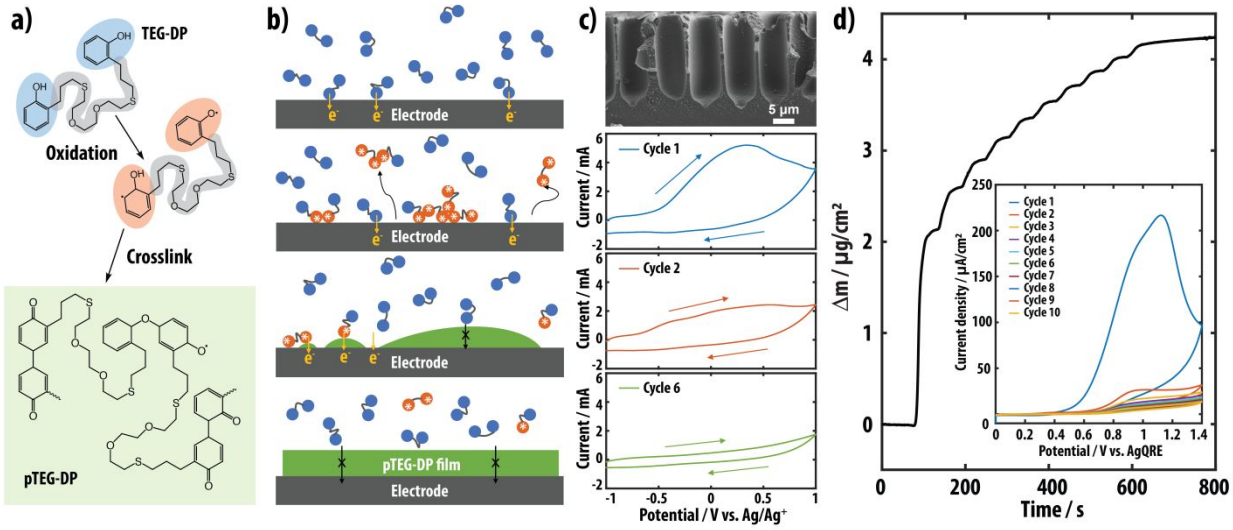

Figure 1. (a) Chemical structures of TEG-DP (phenol end groups are shaded blue), TEG-DP radicals (phenol radicals are shaded orange) and crosslinked poly-TEG-DP (pTEG-DP, green). (b) Scheme of the proposed TEG-DP self-limiting electrodeposition mechanism on an electrode surface. (c) Selected cyclic voltammograms (CVs) of the TEG-DP electrodeposition on a Top: 3D carbon electrode (top: cross-sectional SEM) showing the current change over the deposition stages including initial oxidation, partial passivation, and full passivation with only double-layer current. (d) Mass change during CV-electrodeposition of TEG-DP on a quartz crystal microbalance, each stepwise mass increase corresponds to one CV cycle (inset: corresponding CVs).

Here we report the tunable and conformal electrodeposition of such a dual-functional monomer, triethylene glycol-diphenol (TEG-DP), that combines the conformal film-forming capability of the phenolate ion with the functionality of small oligo(ethylene glycol) derivatives, namely their strong cation solvation for alkaline metal ions.[33] The ultrathin polymerized pTEG-DP films are uniformly applied to planar and porous electrodes alike. A comprehensive determination of their processing-structure-property relationships reveals the broad tunability of the film properties with deposition parameters dictating thickness (7-80 nm), permeability, and electrical properties.

Results and discussion

In order to explore the hypothesis that a versatile film deposition strategy could be achieved by combining an electrodeposition motif and a functional group in a single monomer, we synthesize the dual-functional TEG-DP using UV-initiated thiol-ene coupling of allylphenol and 2,2-(ethylenedioxy)diethanethiol (Figure 1a, Figure S1). The electrochemically active phenolic end groups allow for its oxidative crosslinking into polymer networks by applying an anodic potential to a substrate surface, whose self-limiting film deposition mechanism can be described as 4 steps (Figure 1a,b): (1) By electron transfer to the substrate, the deprotonated phenolate end-groups oxidize to free radicals that (2) couple to dimers and oligo-phenol crosslinks that subsequently (3) deposit onto the surface due to their insolubility at a critical size and (4) stop growing once a critical insulating film thickness is reached that prevents further electron transfer to the phenolic monomers and oligomers.[34,35] The passivating and self-limiting mechanism is expected to yield in full film coverage over the entire electrode surface since areas with lower growth rates, due to lower mass transport or surface activity, continue to grow until reaching the same critical film thickness as that of faster growing areas, even on substrates possessing complex architectures. We demonstrate this fully passivating electrodeposition mechanism of TEG-DP with cyclic-voltammetry (CV) on 3D carbon electrodes with micron-sized cylindrical pores (Figure 1c). During CV electrodeposition, the large current observed in the first cycle at potentials above -0.5 V vs. Ag/Ag^+ corresponding to phenolate oxidation decreases in the second and subsequent cycles to purely double-layer capacitive current, indicating the gradual but complete passivation of the 3D carbon surface with pTEG-DP (Figure 1c). Correspondingly, when TEG-DP is electrodeposited on an electrochemical quartz crystal microbalance (E-QCM), the mass gain during CV-electrodeposition is decreasing stepwise with each cycle and 50% of the final film mass gained within the first cycle, consistent with the depicted mechanism (Figure 1b,d).

To determine their processing-structure-property relationships, we conduct a systematic screening of the electrodeposition parameters of the pTEG-DP thin films on planar indium tin oxide (ITO) coated glass electrodes. Since the electrodeposition potential and the bulk solution concentration of the TEG-DP determine the amount of activated (oxidized) species at the substrate surface, we expect those parameters to most affect the crosslinking kinetics and, thus, the properties of the electrodeposited thin films. To test these processing-dependences, TEG-DP is deposited from a range of concentrations (1, 10, and 50 mM) and constant deposition potentials (E_{dep}) between -0.5 and +0.7 V vs. Ag/Ag^+ for 20 minutes (Figure 2a,b).

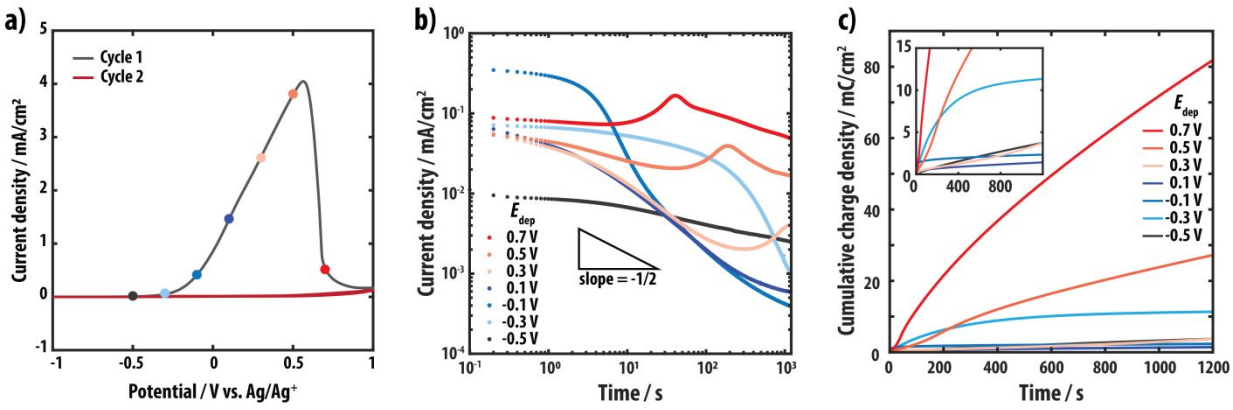

Figure 2. (a) Cyclic voltammetry of TEG-DP on ITO-coated glass. Dots represent the chronoamperometry potentials used in b. (b) Chronoamperometry of the potentiostatic electrodeposition of TEG-DP at the identified E_{dep} vs. Ag/Ag⁺ and (c) temporal evolution of accumulated charge passed during potentiostatic TEG-DP electrodeposition. (a-c) Concentration of TEG-DP is 50 mM with 100 mM TMAH as the base.

Through observation of the current density (j) over time (t) (chronoamperometry or "CA") and determination of the cumulative amount of charge passed during potentiostatic TEG-DP electrodeposition, insight into the oxidation rate and, indirectly, the film formation can be gained (Figure 2b,c, Figure S3). For the tested conditions, three distinct regimes are identified from the CA response.

Regime 1 (no passivation): At E_{dep} < -0.3 V vs. Ag/Ag⁺, the current density decreases by a factor of less than eight over 20 minutes with a slope in the log(j)-log(t) plot above -1/2, indicating an electrochemical reaction determined by a combination of charge-transfer kinetics and mass transfer without surface passivation (Figure 2b, Figures S3a, S4a, S5a).[36] We speculate that the absence of passivation in this regime stems from insufficient kinetics and extent of crosslinking at the surface due to the low local concentration of activated (oxidized) phenol radicals, as indicated by the low amount of charge passed. Additionally, coupled species (oligomers) need to be continuously oxidized at the surface in the presence of other oxidized phenolic species to grow a large enough network for film deposition. Their diffusional loss into the bulk solution before radical coupling prevents further oxidation and growth into a sufficient network size that would form a passivating surface film.

Regime 2 (passivation): At intermediate E_{dep}, the oxidation current decreases rapidly and almost completely ceases after 100 s (Figure 2b, Figures S3b, S4b, S5b). The exact potential range depends on the TEG-DP bulk concentration: for example, at E_{dep} of -0.3 to +0.1 V vs. Ag/Ag⁺ for 50 mM TEG-DP. The charge-time evolution suggests a fast oxidative film growth period that leads to full passivation indicated by its plateauing (Figure 2c, Figures S3b, S4b, S5b). The length of the film growth period and amount of oxidative charge passed depends on the applied potential, with a longer time to reach passivation at lower potentials. At the higher end of this potential range (e.g., E_{dep} = +0.1 V vs. Ag/Ag⁺ for 50 mM TEG-DP), a finite current remains after a fast growth period from slow continued oxidation without further passivation, either due to low but finite molecular permeability of the thin film towards TEG-DP, or it represents the transition to the regime 3 at higher E_{dep}.

Regime 3 (anomalous delayed oxidation): At the highest deposition potentials, for example, at E_{dep} of +0.3 to +0.7 V vs. Ag/Ag⁺ for 50 mM TEG-DP, an unexpected increase in oxidation current is observed at later times, which is not captured with the passivating film deposition mechanism illustrated in Figure 1b. The onset of this current increase is observed at earlier times for higher potentials and this regime appears at lower potentials for higher concentrations. We hypothesize that this additional delayed current is related to the oxidation of oligomeric polyphenol crosslinks with water from the employed base tetramethyl ammonium hydroxide (TMAH $\cdot 5H_2O$) and only occurs after a critical oligo-phenolic size is reached (Figure S7a). To test this hypothesis, TEG-DP is electrodeposited with anhydrous triethylamine with controlled amounts of water (Figure S7b,c). Indeed, an additional delayed current is observed for water concentrations at and above 0.25 M for E_{dep} = +0.2 V vs. Ag/Ag⁺, equivalent to the water concentration in the TMAH system with 50 mM TEG-DP. An earlier onset time and higher current is obtained at increasing water concentrations, while a lower water concentration results in continuously decreasing oxidation current within 100 s, as observed for the fast self-limiting surface passivation (regime 2). In a second test, two pTEG-DP films electrodeposited under anhydrous conditions are subsequently exposed to monomer-free solutions with and without water, respectively, where only the solution with water showed an oxidation current peak after 20 s, in accordance with our hypothesis that the combination of extensive phenolic crosslinking and water are the source of the additional delayed oxidation current (Figure S7d,e).

The distinct electrodeposition and growth regimes are expected to impact the structure and properties of the ultrathin pTEG-DP films. To relate the film growth characteristics under the various deposition conditions to the film topography, their thickness and roughness is determined by atomic force microscopy (AFM) at the film edge and its center, respectively. For pTEG-DP films

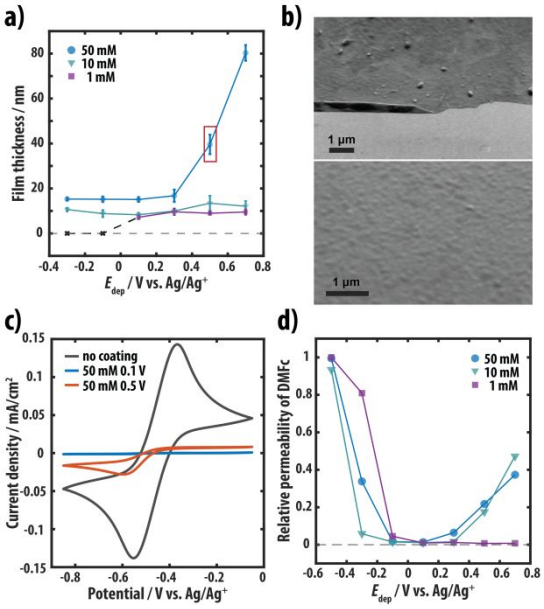

Figure 3. (a) Thickness obtained from AFM of the pTEG-DP films electrodeposited under various conditions (vertical bars denote the roughness, red box indicates sample shown in panel b). (b) SEM images taken at the edge (top) and center (bottom) of the film deposited at +0.5 V vs. Ag/Ag^+ from a 50 mM TEG-DP solution. The folding and debris at the edge if the film is assumed to stem from film delamination during disassembly of the electrodeposition setup and removal of the area-masking O-ring. (c) CVs of decamethylferrocene (DMFc) on bare (black) and pTEG-DP (50 mM) coated ITO electrodes electrodeposited at +0.1 V (blue) and +0.5 V (red) vs. Ag/Ag^+, respectively. (d) Relative permeability to DMFc of the pTEG-DP films electrodeposited under various conditions obtained from the DMFc CV-reduction charge normalized to bare ITO.

from high concentration (50 mM), the thickness is consistent around 15-17 nm at $E_{dep} \leq +0.3$ V vs. Ag/Ag^+, and increases to 40 and 80 nm at +0.5 and +0.7 V vs. Ag/Ag^+, respectively (Figure 3a, Supporting Table S1). In contrast, films obtained from 1 and 10 mM TEG-DP exhibit a consistent thickness of 8-10 nm with only a slight increase to 12-13 nm at $E_{dep} \geq +0.5$ V vs. Ag/Ag^+ for 10 mM TEG-DP (Figure 3a). Consistent with the electrochemical data for regime 1, no detectable films are obtained at $E_{dep} \leq -0.1$ V vs. Ag/Ag^+ for 1 mM TEG-DP. The ultrathin pTEG-DP films exhibit a roughness of less than 2 nm for regime 2 and up to 4 nm for regime 3 electrodeposition. Consistent with AFM, scanning electron microscopy (SEM) corroborates the formation of fully covering and smooth ultrathin films, as shown in Figure 3b for the 40 nm thick pTEG-DP film (50 mM TEG-DP at E_{dep} = +0.5 V vs. Ag/Ag^+). The dependence of the film thickness on both the deposition potential and the monomer bulk concentration provides separate levers for its tailored tunability but is seemingly uncorrelated to the observed delayed oxidation current in regime 3.

Permeability is a performance-determining property of crosslinked polymer materials in functions that depend on mass transport such as controlled absorption and release, sensing, or ion membranes in energy storage and conversion. Molecular permeability is dependent on the effective mesh size of the network. To probe and evaluate the permeability of the electrodeposited pTEG-DP and its correlation to the deposition regimes, we employ decamethylferrocene (DMFc) as an electrochemical probe molecule that exhibits reversible oxidation and reduction around -0.5 V vs. Ag/Ag^+. Using CVs on the electrodes before and after pTEG-DP electrodeposition, uncoated surfaces (no change in CV) can be distinguished from impermeable films (no reduction current) and permeable films (reduced reduction current), as exemplified for films deposited from 50 mM TEG-DP in Figure 3c and summarized for all films in Figure S6. For comparison between the films, we define a relative permeability as the reduction charge density (mC cm^{-2}) from the DMFc CVs normalized by the pre-deposition CV. As expected, an E_{dep} of -0.5 V gives rise to almost full access of the DMFc to the electrode surface implying no or incomplete film formation. Interestingly, a non-monotonic permeability trend is found for films from higher E_{dep}. At moderate E_{dep} between -0.1 V and +0.3 V vs. Ag/Ag^+, fully blocking films are formed with almost no measurable permeability to DMFc. Interestingly, higher $E_{dep} \geq +0.5$ V vs. Ag/Ag^+ for 10 and 50 mM TEG-DP lead to films with increasing relative permeabilities independent of their thickness (Figure 3d), while films obtained from 1 mM TEG-DP remain molecularly impermeable. These results demonstrate that by careful selection of the monomer concentration and deposition potential, the film thickness and molecular permeability can be independently tuned. The films permeability to DMFc indicate that the mesh size and the mobility of the polymer network allows the transport of molecules with comparable and smaller size such as lithium-ion, but the impermeability to DMFc does not indicate that the polymer films prevent smaller ions from passing through.[37,38]

Electronic resistance and dielectric breakdown strength are especially important in the area of energy storage and conversion. To evaluate how these properties depend on the deposition process, the electrodeposited ultrathin pTEG-DP films are characterized by solid-state electrochemical impedance spectroscopy (EIS) and linear-sweep voltammetry using a liquid eutectic gallium-indium (eGaIn) drop as a soft electronic contact to the dry film (Figure 4a).[29] In contrast to the film thickness and molecular permeability, a correlation of the electronic resistance to the presence of the additional delayed oxidation current is identified. In the passivating regime 2, the films exhibit a characteristic parallel-RC circuit behavior with a phase shift of 0 degrees at high and low frequencies and close to -90 degree at intermediate frequencies (Figure 4b) resulting in a semicircle in the Nyquist plot (Figure 4c). The capacitive element originates from the plate capacitor composed of the primary ITO slide, the thin polymer film as a dielectric and the eGaIn electrode. The resistor element in these films stems from the finite electronic resistance of the films, which are in the range of $R = 10^3$-10^4 Ω cm^2 that correspond to material-specific electronic resistivities of $\rho_{el} = 10^9$-10^{10} Ω cm. Interestingly, for films produced in regime 3, which exhibit additional delayed oxidation with water during electrodeposition, an open Nyquist plot and more than one negative peak in the phase shift are observed, representing a more complex equivalent circuit. Importantly, a continuously increasing impedance and phase shift at below -45 degrees with decreasing frequency indicate a high electronic resistance of the pTEG-DP thin films beyond the

measurement limit of the EIS instrument ($R > 10^6$ Ω cm^2 and ρ_{el} > 10^{11} Ω cm). From linear-sweep voltammetry, a resistance of 3 × 10^6 Ω cm^2 is determined for the films deposited in regime 3 ($\rho_{el} > 7 \times 10^{11}$ Ω cm). The additional delayed oxidation current in deposition regime from the oxidation of the polyphenolic

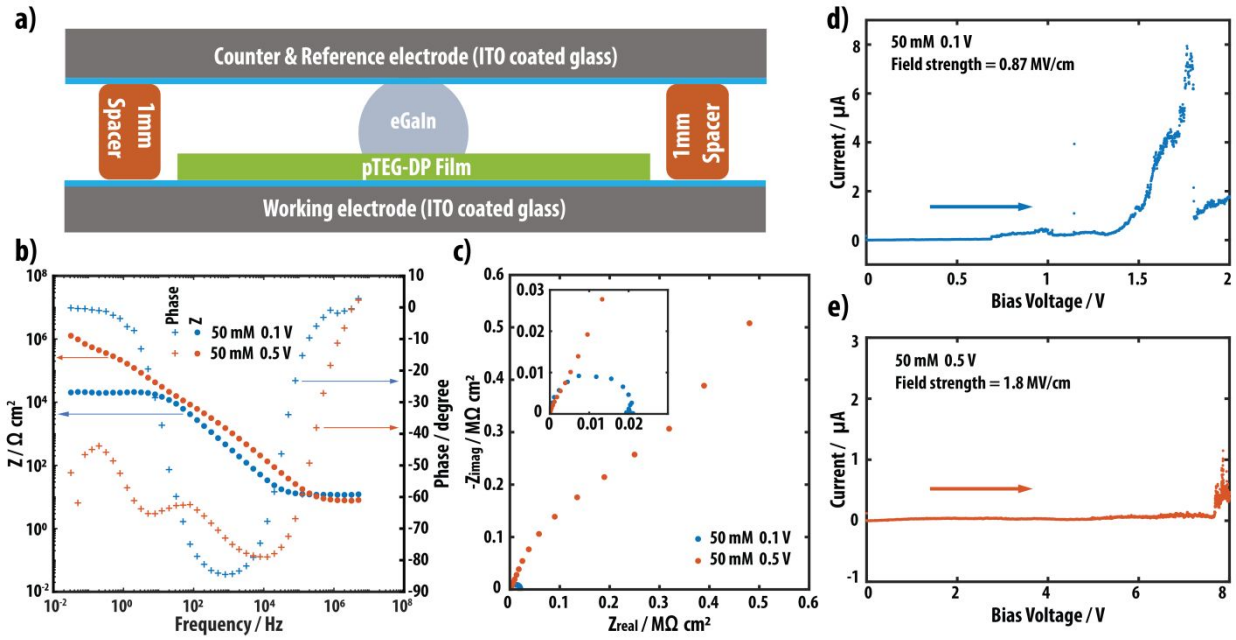

Figure 4. (a) Setup for solid-state film EIS measurement and dielectric breakdown measurement. (b) Bode plot and (c) Nyquist plot of films deposited at two chosen conditions (50 mM TEG-DP solution, +0.1 V and +0.5 V vs. Ag/Ag$^+$). (d, e) Dielectric breakdown measurement films deposited in 50 mM TEG-DP solution at +0.1 V and +0.5 V vs Ag/Ag$^+$ respectively.

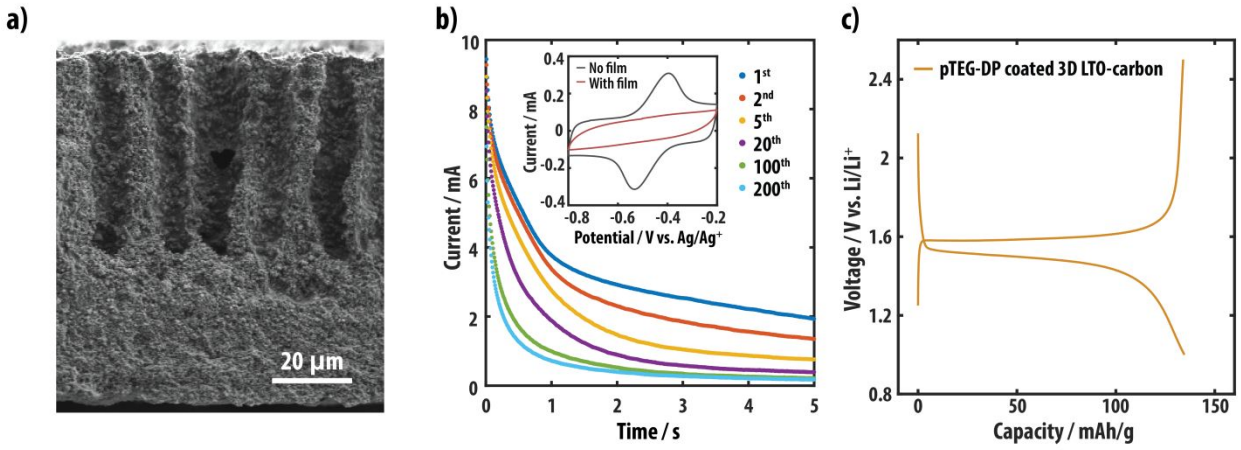

Figure 5. (a) Cross-sectional SEM image of 3D LTO-carbon composite electrode. (b) Selected CA traces of the potentiostatic electrodeposition from 50 mM TEG-DP at +0.1 V vs. Ag/Ag$^+$ on the 3D LTO-carbon electrode. Inset: DMFc CVs before and after electrodeposition. (c) Charge and discharge curves (5th cycle) of pTEG-DP coated 3D LTO-carbon electrode (9.1 mA/g, 0.05 C based on the theoretical LTO capacity of 175 mAh/g), demonstrating lithium permeation through the pTEG-DP film.

crosslinks with water could remove electronic conjugation throughout the polyphenolic network and yield higher electronic insulation, a hypothesis consistent with the observed increase in electronic resistance. The more complex EIS response of these films is likely caused by trapped electrolyte ions in the molecular network due to the high permeability generating an additional double-layer capacitor element in the complex equivalent circuit. For comparison between the electrodeposited pTEG-DP films, the impedance at the lowest frequency is listed in Table 1. As is evident, the large impedance of films from the higher monomer concentrations (10 mM and 50 mM) and high E_{dep} is not simply due to the ohmic resistance that scales with the increasing film thickness, but due to an increase of material-intrinsic resistivity. A similar electronic

resistivity was previously reported for purely dielectric poly(phenylene oxide) (PPO) thin films of 21 nm thickness (10^{11} Ω cm) electrodeposited at high potentials.[29]

Since the electric field strength scales with the dielectric film thickness in thin-film capacitors, and electrochemical stability is crucial for artificial battery interphases, the breakdown voltage of the ultrathin pTEG-DP films and its dependence on the deposition parameters is of practical importance for energy storage applications. Using linear-sweep voltammetry with the same liquid eGaIn contact, the breakdown voltage of films electrodeposited at +0.1 V and +0.5 V vs. Ag/Ag+ (50 mM TEG-DP) is determined as the potential where the current deviates from a linear regression fit at 1.4 V and 7.6 V, corresponding to a dielectric breakdown strength of 0.87 MV cm^{-1} and 1.8 MV cm^{-1}, respectively (Figure 4d). The latter value is comparable to the previously reported dielectric strength of an electrodeposited PPO thin film obtained from pure phenol oxidation, however, with a higher absolute voltage stability.[29] Hence, our results demonstrate that when deposited at high potentials, the electrodeposited pTEG-DP films exhibit the good dielectric properties of PPO thin films while also providing a high degree of permeability, potentially enabling their use as advanced artificial interphases in energy storage and sensing applications.

Table 1. Low frequency impedance / Ω cm²

E_{dep} / V vs. Ag/Ag$^+$	Bulk concentration		
	50 mM	10 mM	1 mM
-0.3	4×10^3	8×10^2	2×10^3
-0.1	1×10^3	4×10^4	1×10^5
0.1	2×10^4	2×10^4	$>10^6$
0.3	5×10^4	5×10^4	3×10^5
0.5	$>10^6$	$>10^6$	2×10^3
0.7	$>10^7$	$>10^6$	4×10^2

To evaluate the stability and applicability of a pTEG-DP interphase in an energy storage application, we electrodeposit pTEG-DP on a free-standing 3D-structured lithium-ion battery electrode composed of 80 wt% lithium titanate (LTO) and 20 wt% carbon with straight low-tortuosity channels perpendicular to the electrode and 7~10 μm in diameter (Figure 5a) using hybrid inorganic phase inversion method[39]. To ensure consistent monomer concentration in the micron-sized pores and accommodate slower diffusion in the 3D-structure electrode, repeating potentiostatic deposition is employed with 5 s applied deposition potential and 10 s rest intervals for diffusional TEG-DP replenishment in the pores (50 mM TEG-DP, E_{dep} = +0.1 V vs. Ag/Ag$^+$). During the deposition, the anodic current decreases significantly with increasing deposition pulse number, and eventually exhibits almost exclusively double-layer current (Figure 5b). The passivation of the entire 3D LTO-carbon electrode surface is demonstrated by the absence of DMFc redox peaks during CV (Figure 5b, inset). The pTEG-DP coated LTO-carbon electrode is assembled into a liquid-electrolyte half-cell and galvanostatically charged and discharged. Though the p(TEG-DP) film increased the cell resistance by approximately 580 Ω (Figure S10), the coated electrode still exhibits stable and flat (dis)charge plateaus with small overpotential, indicating that the pTEG-DP film allows lithium-ion transport between the liquid electrolyte and the solid electrode (Figure 5c).

Conclusions

Here we report the rational design and electrodeposition of a dual-functional molecular architecture with phenol end-groups for conformal electrodeposition and a functional molecular core of triethylene glycol. We demonstrate a non-monotonic interrelation between the deposition parameters and the film properties that can be classified into two groups: (1) films that are thin, impermeable, and exhibit finite electronic resistance are obtained at moderate deposition potentials or at low monomer concentrations, and (2) permeable, electronically insulating films whose thickness is tunable by the monomer concentration during deposition are formed at higher potentials and concentrations, though electronic resistance is further tunable by the water content. We anticipate that our concept is directly applicable to the electrodeposition of other phenol-modified monomers for uniform ultrathin coatings and interphases of various functionalities and that the demonstrated processing-structure-property relationships will enable precisely tailored designer interphases in future energy storage solutions.

Author Contributions

The manuscript was written through contributions of all authors. All authors have given approval to the final version of the manuscript. WW conducted the experiments on the electrodeposition and characterization of pTEG-DP films. ZZ aided in the synthesis of TEG-DP and conducted the experiments on the effect of water. AR fabricated the 3D carbon and LTO–carbon electrodes and performed battery tests. JGW and KAB devised the original idea and supervised this project. WW and JGW wrote the manuscript. All authors have given approval to the final version of the manuscript.

Conflicts of interest

The authors declare no competing financial interest.

References

1 J. J. Licari, *Coating Materials for Electronic Applications: Polymers, Processing, Reliability*, *Testing*, Noyes Publications / William Andrew, Inc., Norwich, NY, 2003.
2 H. Ito, in *Chemical Amplification Resists for Microlithography*, Microlithography· Molecular Imprinting, **2005**, 37-245.
3 O.-K. Kwon, J.-S. An and S.-K. Hong, *IEEE Sens. J.*, **2018,** 18, 4832-4846.
4 J. Ciosek, in *Corrected Color Glasses for Effective Protection of Eyes*, Optical Sensing for Public Safety, Health, and Security, SPIE, **2001**, pp. 30-34.

5 T. P. Russell and Y. Chai, *Macromolecules*, **2017,** 50, 4597-4609.
6 O. K. Tsui and T. P. Russell, *Polymer Thin Films*, World Scientific, Singapore, 2008.
7 G. Crabtree, J. Sarrao, P. Alivisatos, W. Barletta, F. Bates, G. Brown, R. French, L. Greene, J. Hemminger and M. Kastner, *From Quanta to the Continuum: Opportunities for Mesoscale Science*, USDOE Office of Science (SC), United States, 2012.
8 J. C. Hemminger, J. Sarrao, G. Crabtree, G. Flemming and M. Ratner, *Challenges at the Frontiers of Matter and Energy: Transformative Opportunities for Discovery Science*, USDOE Office of Science (SC), United States, 2015.
9 A. Pearse, T. Schmitt, E. Sahadeo, D. M. Stewart, A. Kozen, K. Gerasopoulos, A. A. Talin, S. B. Lee, G. W. Rubloff and K. E. Gregorczyk, *ACS Nano*, **2018,** 12, 4286-4294.
10 S. N. Abdollahi, E. O. Martínez, C. Kilchoer, G. Kremer, T. Jaouen, P. Aebi, T. Hellmann, T. Mayer, Y. Gu and U. B. Wiesner, *Adv. Mater. Interfaces*, **2020,** 7, 2001227.
11 A. M. Urbas, Z. Jacob, L. Dal Negro, N. Engheta, A. Boardman, P. Egan, A. B. Khanikaev, V. Menon, M. Ferrera and N. Kinsey, *J. Opt.*, **2016,** 18, 093005.
12 T. S. Arthur, D. J. Bates, N. Cirigliano, D. C. Johnson, P. Malati, J. M. Mosby, E. Perre, M. T. Rawls, A. L. Prieto and B. Dunn, *MRS Bulletin*, **2011,** 36, 523-531.
13 J. G. Werner, G. G. Rodriguez-Calero, H. D. Abruna and U. Wiesner, *Energy Environ. Sci.*, **2018,** 11, 1261-1270.
14 G. Ramesh, S. Porel and T. Radhakrishnan, *Chem. Soc. Rev.*, **2009,** 38, 2646-2656.
15 L. Ma, Z. Xu, Y. Chen, M. Zhang, J. Yin, M. Li, K. Chen and P. Yin, *ACS Appl. Mater. Interfaces*, **2020,** 12, 38655-38661.
16 S. Bonfanti, R. Guerra, F. Font-Clos, D. Rayneau-Kirkhope and S. Zapperi, *Nat. Commun.*, **2020,** 11, 1-10.
17 S. H. Baxamusa and K. K. Gleason, *Chem. Vap. Deposition*, **2008,** 14, 313-318.
18 D. Belanger and J. Pinson, *Chem. Soc. Rev.*, **2011,** 40, 3995-4048.
19 B. Zdyrko and I. Luzinov, *Macromol. Rapid Commun.*, **2011,** 32, 859-869.
20 A. Olivier, F. Meyer, J.-M. Raquez, P. Damman and P. Dubois, *Prog. Polym. Sci.*, **2012,** 37, 157-181.
21 J. B. Schlenoff and G. Decher, *Multilayer Thin Films: Sequential Assembly of Nanocomposite Materials*, John Wiley & Sons, Weinheim, Germany, 2006.
22 Y. Cho, W. Lee, Y. K. Jhon, J. Genzer and K. Char, *Small*, **2010,** 6, 2683-2689.
23 G. Decher, *Thin Solid Films*, **1992,** 210, 831-835.
24 T. Serizawa, S. Kamimura, N. Kawanishi and M. Akashi, *Langmuir*, **2002,** 18, 8381-8385.
25 S. Komaba and T. Osaka, *J. Electroanal. Chem.*, **1998,** 453, 19-23.
26 D. Hu, C. Peng and G. Z. Chen, *ACS Nano*, **2010,** 4, 4274-4282.
27 R. L. McCarley, R. E. Thomas, E. A. Irene and R. W. Murray, *J. Electroanal. Chem. Interfacial Electrochem.*, **1990,** 290, 79-92.
28 M. Ferreira, H. Varela, R. M. Torresi and G. Tremiliosi-Filho, *Electrochim. Acta*, **2006,** 52, 434-442.
29 C. P. Rhodes, J. W. Long, M. S. Doescher, J. J. Fontanella and D. R. Rolison, *J. Phys. Chem. B.*, **2004,** 108, 13079-13087.
30 C. P. Rhodes, J. W. Long, K. A. Pettigrew, R. M. Stroud and D. R. Rolison, *Nanoscale*, **2011,** 3, 1731-1740.
31 M. Y. Timmermans, F. Mattelaer, S. Moitzheim, N. Clerckx, A. Sepulveda, S. Deheryan, C. Detavernier and P. M. Vereecken, *J. Appl. Polym. Sci.*, **2017,** 134, 44533.
32 D. J. Bates, C. M. Elliott and A. L. Prieto, *Chem. Mater.*, **2014,** 26, 5514-5522.
33 N. Hasan, M. Pulst, M. H. Samiullah and J. Kressler, *J. Polym. Sci. Part B: Polym. Phys.*, **2019,** 57, 21-28.
34 M. Gattrell and D. Kirk, *J. Electrochem. Soc.*, **1992,** 139, 2736.
35 M. Gattrell and D. Kirk, *J. Electrochem. Soc.*, **1993,** 140, 903.
36 A. J. Bard, L. R. Faulkner and H. S. White, *Electrochemical Methods: Fundamentals and Applications*, John Wiley & Sons, 2022.
37 D. P. Freyberg, J. L. Robbins, K. N. Raymond and J. C. Smart, *J. Am. Chem. Soc.*, **1979**, 101, 892–897
38 P. F. Lang and B. C. Smith, *Dalton Trans.*, **2010**, 39, 7786–7791
39 A. B. Resing, C. Fukuda and J. G. Werner, *Adv. Mater.*, **2022**, 2209694.